Numerical Analysis of Defects in FML using Through-Transmission Mode of Active Thermography

S.Sundaravalli[#1], M.C.Majumder[2], G.K.Vijayaraghavan[3]

[#1]*Department of Mechanical Engineering, Roever College of Engineering and Technology, Perambalur, India 621212*

[2]*Department of Mechanical Engineering, Roever Engineering College, Perambalur, India 621212*

[3]*National Institute of Technology, Durgapur, India 713 209*

Abstract— **The study mainly focuses to investigate the thermal response of defects such as delaminations and disbonds, and develop mathematical models using numerical results to obtain the optimum heat requirement and time to identify defects in GLARE type of Fibre metal laminates (FML) under a through-transmission (TT) mode of step pulsed active thermography (SPAT) method in the type of nondestructive testing and evaluation (NDTE) technique. The influence of applied heat flux and time on various sizes and depth of defects in FML is analysed to investigate the thermal response through numerical simulations. A finite element method (FEM) is applied to simulate SPAT through ANSYS software based on 3D transient heat transfer principle with the assumption of TT mode of observation.**

The investigation shows that the smaller and near-surface defects located at the thermal stimulant side respond with reduced thermal contrast and vice versa. Numerical results are analysed to provide the optimum heat requirement and time to identify defects at the required MRTD even to identify defects which are not identified within the load conditions considered for the investigations.

Further, a comparative study concludes that the numerical approach based on SPAT using TT mode of observation could be utilized to derive mathematical models using numerical results to analyse defects present in FML effectively.

***Keywords*— Step pulsed active thermography (SPAT), Through-transmission mode (TT), NDTE, FML, Delaminations, Disbonds, Finite element method, Thermal contrast.**

I. INTRODUCTION

In olden days, aircraft panels were made of metallic materials, such as aluminum, titanium, beryllium etc. They led to increase fuel consumption due to increased weight. Then, the concept of effective and efficient usage of materials in manufacturing of aircraft panels was slowly emerged by using alloys of aluminum, titanium and beryllium with reduced weight and cost. Inherent complexity in manufacturing such alloys led researchers to move from metallic materials to composite materials. The composite materials play an important role in heavy duty applications because of reduction in weight and cost-effective. The use of composite materials in manufacturing of aircraft panels was alike alloys of metallic materials. First time, in 1980s, the Delft University of Technology developed a new type of composite called Fibre Metal Laminates (FML) for making aircraft panels [1].

Defects may be produced either during manufacturing of FML or bonding composite layers with aluminum sheets, handling, or under service conditions. Defects include air gap (disbonds) and foreign particles inclusions (intrusion), fibre misalignment, fibre failure, thickness variations, delaminations etc. [4]. Disbonds and delaminations between composite layers are common defects in many of aircraft panels manufacturing industries. A proper assessment of such defects is essential as they may have adverse effects on the performance and safe operation of aircrafts. Usually, these anomalies are identified and characterized by various non-destructive testing and evaluation (NDTE) techniques. Infrared thermography (IRT) is one of several NDTE techniques and it essentially uses the abnormal temperature distribution on the surface of the specimen to detect and characterize defects present in composite structures [18].

Thermography is a non-destructive, non-contact and non-intrusive inspection technique that involves mapping of surface temperatures distribution of the structure to assess the subsurface features of the structure or behaviour of the system. Thermography has been successfully applied over the decades to evaluate the integrity of materials, joints, electrical connections in a wide range of industrial as well as in detection of defects, such as delaminations and disbonds in layered structures, hidden corrosion in metallic components, cracks in ceramics and metals, voids, impact damage and inclusions in composite materials [14], [20], [9], [13].

II. LITERATURE REVIEW

Fibre metal laminates are a new family of hybrid materials consisting of thin metal layers bonded together by fibres embedded in an adhesive [7]. As a result of this build-up, FML possess a mixture of the characteristics of both metals and FRP materials. A GLARE is a GLAss- REinforced composite in the type of FML which was mainly used in Airbus A380 super jumbo in 2001. The internal flaws called defects are invisible on the surface of the structure which may

be produced during manufacturing, handling and under service conditions which may lead to unavoidable accidents. Therefore, a proper assessment of defects is required to make them use safely. Under many literature reviews, some of thermographic investigations were carried on FMLs, such as nondestructive evaluation of damage assessment in FMLs using ultrasonic and eddy current inspection [4], the influence of cooling rate on the fracture properties of a thermoplastic-based FMLs [6], applications of an aluminum–beryllium composite for structural aerospace components [24], modelling of FML for simulation of the inter rivet buckling behaviour in a stiffened fuselage shell [21]. The numerical results were compared to the experimental data both qualitatively and quantitatively, non-destructive evaluation of aerospace materials with lock-in thermography [15], numerical modeling for thermographic inspection of FMLs by both flash pulsed and lock-in thermography [13] and the influence of disbond damage on Lamb wave propagation in GLARE composites [22].

A two dimensional (2D) finite element modeling (FEM) was used for analysing the delamination parameter effects in a composite flat plate setup in which the delaminations were produced using Teflon and other artificial inserts [11]. The possibility of identifying the defect type was demonstrated in complex structure CFRP samples inspected by thermography using experimental and FEM results [16]. The usefulness of IRT technique was shown in detecting the subsurface disbonds prior to maintenance and rehabilitation work [8]. They investigated the use of finite element (FE) heat transfer modeling to predict IRT images from GRP bridge decks with subsurface disbonds by measuring thermal properties of the GRP bridge deck and the wearing surface, and heat transfer FE modeling of decks with disbonds of different thicknesses. The author applied both pulsed and lock-in thermography for the detection of delaminations in FML made by E-glass fibre and Aluminium metal laminates using combined experimental and FEM approach [13]. The researcher conducted experiments on GRP pipes for analysing delaminations using step pulsed active thermography (SPAT) [27]. The active thermography approaches, such as pulsed thermography and vibrothermography were employed in order to detect simulated delamination (inserts), as well as impact damage on GLARE composite panels [10]. The investigative reports arrived from above mentioned literatures concluded that the thermography could be used in the rapid investigation of GLARE composites, producing interpretable results.

Few works, such as [17] and [27] were only reported on SPAT method under reflection mode for analysing GRP pipes. The above-mentioned literatures show that SPAT of IRT is an effective tool for detecting delaminations in GRP pipes. The researcher [25] presented results from a study aimed at developing a novel thermochromic liquid crystal (TLC) temperature measurement system that uses light transmission instead of light reflection to measure surface temperature fields. The author [20] aimed to develop a non-destructive tool for the evaluation of bonded plastic joints. The paper examined IRT of both transmission and reflection modes imaging and validated the feasibility of the thermal NDT approach for this application. The results demonstrated a good estimation performance for adhesion integrity, uniformity and bond strength using a transmission mode application of IRT. The results of transmission mode were shown to provide greater accuracy over the reflection mode in defect depth estimation. The research [26] was presented a novel way to inspect local wall thinning in metal tubes with IRT both numerically and experimentally. The numerical analyses were carried out in both transmission and reflection modes using simulations. Also, experiments in through-transmission (TT) mode alone were carried out based on the trends and features that emerged from the model. This new concept of TT mode of SPAT led the author to apply in FML for investigating defects. In addition, it was found that no indicative work was carried out on FML aircraft structures under TT mode of SPAT using a FEM for analyzing defects, such as delaminations and disbonds. Hence, the current study focuses to analyse the effect of size and depth of both delaminations and disbonds on applied heat flux with time using SPAT method and develop mathematical models from numerical results to obtain the optimum heat requirement (q) and time to identify defects (T).

In SPAT method**,** the heat pulse is applied on the surface of the specimen for longer time duration, normally a few seconds [14] for the effective investigation of defects. The thermal contrast (ΔT) at specific time during heating was numerically obtained for analysing the thermal response of delaminations and disbonds. ΔT is the temperature difference between non-defective region over defective region. The maximum resolvable temperature difference (MRTD) for the most of the available thermal imager (IR camera) is around $0.1^{o}C$ [3] which is chosen as a threshold value for this analysis to investigate/identify the defects in FML structures. Therefore, MRTD value of $0.1^{o}C$ is set as the required threshold ΔT as the justification factor for investigating defects.

III. METHODS OF IRT

IRT techniques are classified into two types based on the temperature difference produced to obtain thermal image: passive thermography and active thermography. In a passive thermography, no external heat stimulant is used to produce sufficient surface temperature difference for analysing the abnormality present in FML aircraft structure. The temperature difference naturally exist in the structure is used to analyse defects. In an active thermography, an external energy is applied to generate meaningful ΔT that will yield to identify subsurface defects [4]. This energy can be either thermal or mechanical and can be deployed using different ways, such as flash heating, step heating, lock-in thermography (LT) and vibro-thermography (VT). SPAT is a kind of active thermography using step heating which was pioneered by Milne and Reynolds in the early 1980s, developing earlier work that has established the value of infrared techniques for delaminations and disbonds analysis [23]. In this technique, a continuous heat flux is applied on a

specimen by a powerful lamp and the observation of thermal wave heat intensity reaching the rear surface of the specimen. The surface temperature of defective and non-defective regions is recorded by an infrared thermal imager/infrared camera to obtain ΔT for the result analyses.

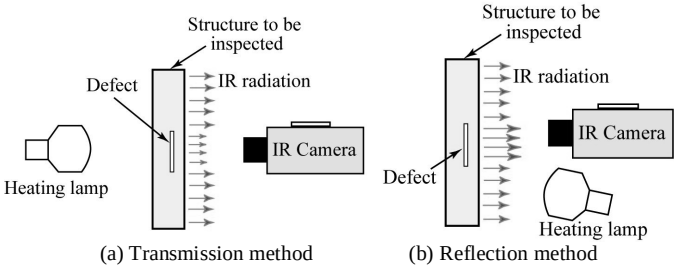

Fig 1. Methods of IRT

There are two common schemes of SPAT: thermal reflection and thermal through-transmission. In the former method, the heat source and IR camera are situated at the same side and the reflected thermal wave effect on the surface temperature is continuously monitored. The latter one needs to access the back surface of the sample that is not possible in many practical cases, such as the sample with curved boundaries *in situ*. In the thermal reflection mode, both the camera and heating sources are located on the front side [12]. Figure 1 (a) and figure (b) depict the basic principle of through-transmission and reflection methods of observations. In this study, delaminations and disbonds in FML aircraft structure are analyzed by SPAT under TT mode.

IV. Numerical Modelling

FEM is mostly used to simulate thermal behaviour of materials containing defects, such as delaminations and disbonds. FEM is a powerful numerical tool that enables the solution of complex nonlinear, non-symmetrical mathematical problems governed by partial differential equations, such as one of heat transfer by conduction, convection and radiation with temperature dependent thermal properties of material involved [16].

For this study, the transient heating of FML structure with delaminations and disbonds of varying sizes at various depths was numerically simulated using FEM to observe the thermal response of applied heat flux with time. FEM simulations were carried out using the ANSYS package.

A. Model of FML Structure and Material Properties

For this study, a FML was modelled with three glass-fibre reinforced epoxy (GRE) laminates of 200×115×0.15mm placed one over the other bonded between the aluminum laminates of 200×115×0.3mm of one at the top and the other one at the bottom. A model 1 was considered for modeling defects in FML with the assumption of artificially induced Teflon film delaminations of 0.045 mm thick. They are numbered from 1 to 6 locating at 0.45mm depth in the thermal stimulator side and delaminations from 7 to 12 are numbered for the location at 0.6mm depth, as shown in figure 2. The model 2 was considered for modeling disbonds with the same dimensions of delaminations which are numbered from 13 to 24, as shown in figure 3.

TABLE I

DIMENSIONS OF DELAMINATIONS AND DISBONDS

Delamination and disbond No.	**Size, mm**	**Depth, mm (from base)**
1,13	2.5×2.5	0.45
2,14	5×5	0.45
3,15	7.5×7.5	0.45
4,16	10×10	0.45
5,17	12.5×12.5	0.45
6,18	15×15	0.45
7,19	2.5×2.5	0.6
8,20	5×5	0.6
9,21	7.5×7.5	0.6
10,22	10×10	0.6
11,23	12.5×12.5	0.6
12,24	15×15	0.6

Table 2 shows the thermal properties of Al 2024-T3, GRE, Teflon and air taken from the literatures [13], [7], [27]. The properties of GRE are taken for the fibre volume fraction of 60% which is most commonly used for GRE composite materials.

TABLE II

THERMAL PROPERTIES OF AL 2024-T3, GRE, TEFLON AND AIR

Properties	**Thermal conductivity (W/m^{o}C)**	**Specific heat (J/kg^{o}C)**	**Density (kg/m^3)**
Al 2024-T3	121	875	2780
Glass-fibre epoxy at 0^o Fibre orientation	0.845	840	1960
Glass-fibre epoxy at 90^o Fibre orientation	0.48	840	1960
Teflon	0.252	1043	2150
Air	0.0263	1005	1.2

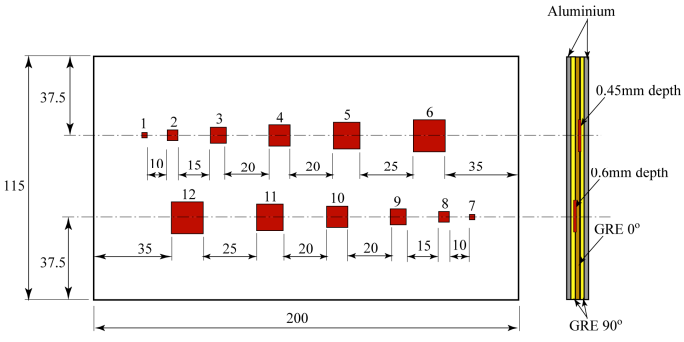

Fig. 2 A model 1

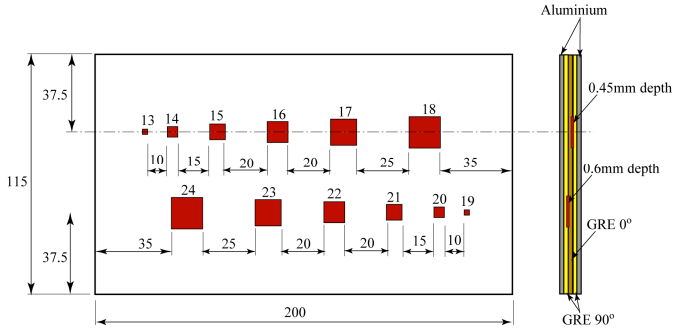

Fig. 3 A model 2

B. Element Description

The model was meshed using 3D thermal solid elements. 8-node quadrilateral elements were used. In particular, SOLID70 elements were selected from ANSYS library. The reason of selecting SOLID70 is that 8-node elements have compatible temperature shapes. 8-node thermal element is applicable to a 3D, transient thermal analysis [2]. In order to obtain a good description of the heat transfer process around defects, mapped meshing was used instead of automatic meshing to create a fine mesh at defective regions.

C. Loading and Boundary Conditions

The front surface of FML was subjected to a uniform q ranging from 10000 W/m^2 to 20000W/m^2. The rear surface of the model was retained to convection boundary with a convection heat transfer coefficient of h = 10W/m^{2}K [19]. The ambient temperature was set at 28^{o}C. The side surfaces of the model were considered to be adiabatic under TT mode of observation [3]. The differences resulting from applying the radiation conditions was so small as to not affect the surface in any quantifiable manner. Therefore, the effects of radiation and convection can be ignored [11].

V. Results and Discussions

The temperature of the defect at the rear side of thermal imager, such as delaminations and disbonds was measured at the centre of the defective region but the vicinity of the defects was measured for non-defective region. ΔT curves were used for the analysis during step heating in TT mode obtained through simulations at specific intervals. The investigations were based on the thermal response, such as thermal contrast (ΔT) and time (t) to attain the required MRTD with applied (q).

A. Analysis of Delaminations

1) Effect of Delamination Sizes on Applied Heat Flux: The results shown in Figure 4 illustrate that ΔT of delaminations from 1 to 6 varies with time for various sizes when q of 16000W/m^2 is applied. During the initial period, ΔT increases nonlinearly with time and it remains almost constant thereafter. ΔT curves are similar and shifted one above the other for delaminations from1 to 6. The reason is that the larger delaminations produce more thermal barrier above delamination surface due to wide area of delaminations. Due to this, the surface below delaminations is less warmed by reducing its surface temperature which leads to increase in ΔT. It is also inferred that larger delaminations need less applied q to attain the required MRTD of 0.1^{o}C as ΔT for the identification of delaminations. The delamination 1 produces a maximum ΔT of 0.0642^{o}C which is insufficient to identify it.

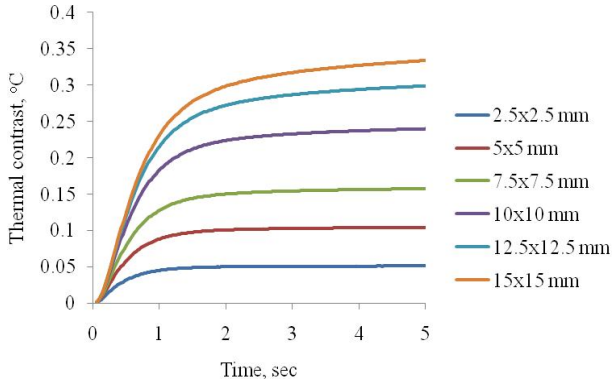

Fig. 4 Thermal contrast curves for delaminations 1 to 6 with time for 16000W/m^2

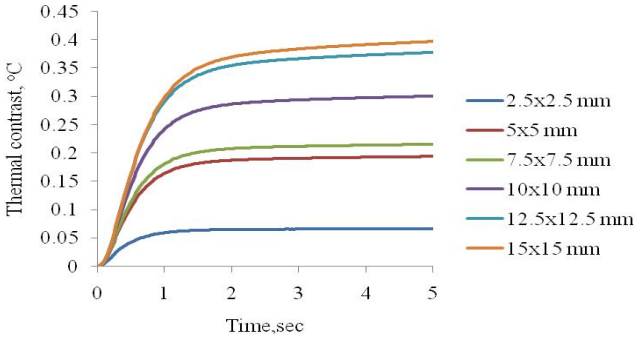

Fig. 5 Thermal contrast curves for delaminations 7 to 12 with time for 16000W/m^2

Figure 5 indicates that ΔT increases nonlinearly with time for the first 2sec and it remains almost constant with slight instability thereafter for delaminations from 7 to 12 when q of 16000W/m^2 is applied. In this case also, the thermal contrast curves are shifted one above the other but the pattern of ΔT curves do not follow the same pattern of delaminations from 1 to 6. It is due to the change in thermal conductivity of GRE at 0^o fibre orientation because the delaminations 1 to 6 are located at GRE 90^o fibre orientation, as shown in figure 2. The value of ΔT for delaminations from 7 to 12 is slightly more when compared to delaminations 1 to 6, as shown in Figure 5. The reason for more ΔT is that the distance covered by thermal waves after passing through delaminations reaching the rear surface is less than the distance covered by delaminations from 1 to 6. Hence, the thermal waves reaching the thermal imager at the rear surface are faster thereby leading to increase the surface temperature.

2) Comparison of Delaminations at Various Depths: Figure 6 shows the comparison between delaminations located at 0.45mm and 0.6 mm depth. It is observed that the deeper delaminations produce more ΔT than near-surface delaminations in TT mode due to above-mentioned reason to figure 5. For example, the delamination 4 produces 0.1831°C at 1 sec with the applied q of 16000 W/m^2 but 0.2424°C is produced by delamination 10 with the same q and time.

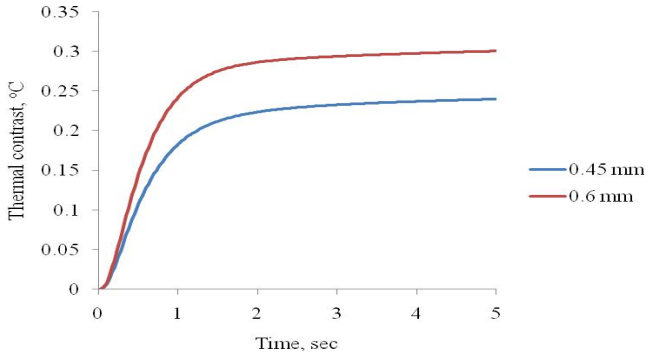

Fig. 6 Comparison of thermal contrast curves with time for delaminations 4 and 10

3) Effect of Applied Heat Flux on Fixed Delamination Size: The results shown in Figure 7 illustrate that ΔT for delamination 3 varies with time for various applied q.

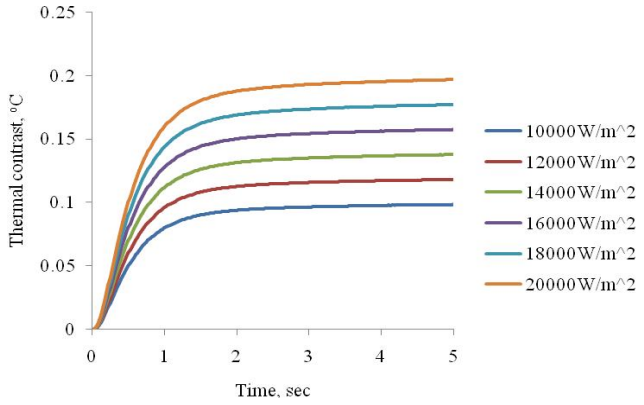

Fig. 7 Thermal contrast curve of delamination 3 with time for various applied heat fluxes (q)

ΔT curves are similar and equi-spaced one above the other due to constant increase in applied q. It is observed that delamination 3 produces less ΔT with 10000W/m^2 but it is more when 20000W/m^2 is applied.

Figure 8 shows ΔT for delamination 9 in which ΔT curves are equi-spaced and they follow the similar pattern of delamination 3 due to the same reason mentioned to figure 7. The results of delaminations 3 and 9 conclude that Δ*T* of delaminations is directly proportional to the applied q as per Fourier's law of heat conduction. The above investigations illustrate that q required for producing sufficient MRTD to identify delaminations is mainly based on the applied q, time, depth and size of delaminations.

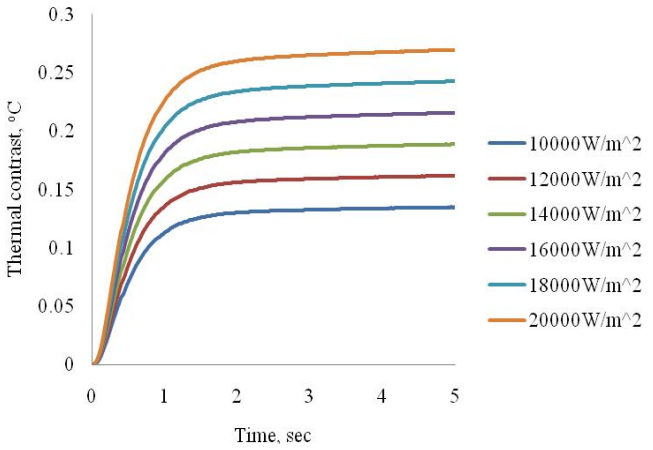

Fig. 8 Thermal contrast curve of delamination 9 with time for various applied heat fluxes (q)

4) Heat Requirement Analysis on Delaminations: Figure 9 shows that ΔT at 1 sec for delaminations from 1 to 6 varies linearly with applied q. From results, it is observed that delamination 1 does not attain the required MRTD with the maximum applied heat of 20000W/m^2 but the delaminations from 2 to 6 produce sufficient MRTD for the delamination identification. Therefore, the delamination 1 could not be identified within the load conditions considered in this study or it might be identified by applying further more q.

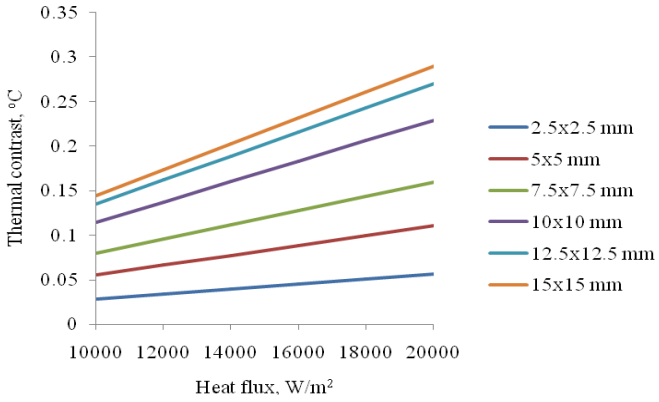

Fig. 9 Thermal contrast curve of delaminations 1 to 6 with q at 1sec

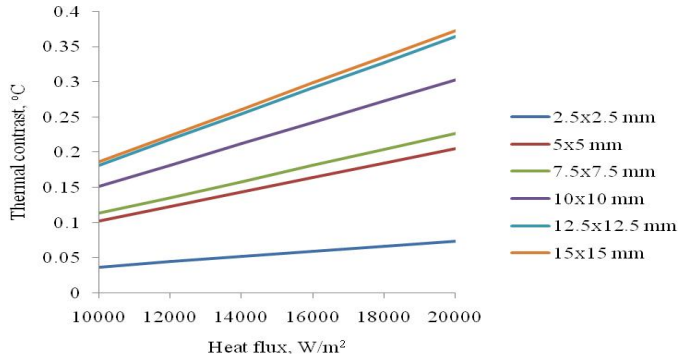

Fig. 10 Thermal contrast curve of delaminations 7 to 12 with q at 1sec

Figure 10 shows that ΔT at 1 sec for delaminations from 7 to 12 varies linearly with applied q. From results, it is observed that delaminations from 7 to 12 produce sufficient MRTD. From figure 9 and figure 10, it is inferred that delamination 1 could not be identified but all delaminations located at 0.6 mm depth could be easily identified within the load conditions considered in this analysis.

For the effective utilization of SPAT of TT mode, the development of a mathematical model using extracted numerical results from simulations is essential to resolve this problem to find the optimum heat requirement for unidentified delaminations. Therefore, the optimum heat requirement could be derived through heat requirement analysis by generalized equations for 0.45mm and 0.6mm depth individually.

The optimum heat requirement equation for delaminations 1 to 6 could be obtained by:

$$q = -1899872000000.07s^4 + 58880906666.65s^3 - 415029800s^2 - 2157025.67s + 33189.05 \quad (1)$$

The optimum heat requirement equation for delaminations 7 to 12 could be obtained by:

$$q = -13317333333.33s^3 + 499268571.43s^2 - 6156938.10s + 29961.6 \quad (2)$$

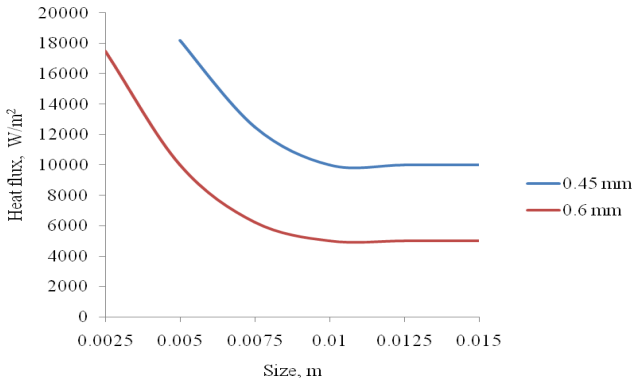

Fig. 11 Compariosn of optimum q requirement for delamiantions 1 to 6 and 7 to 12

From above equations, the optimum q is calculated for the delamination 2 as 18200.87W/m^2 and delamination 6 requires 9994W/m^2 to identify the presence of delaminations. The optimum q of 9993.96W/m^2 and 4996.96W/m^2 are required to identify delaminations 8 and 12 respectively, as shown figure 11. It is understood that delaminations 2 and 8 are smaller than delaminations 6 and 12 respectively. From results arrived by comparison, the smaller and near-surface delaminations need more q to reach MRTD than larger and deeper delaminations. The optimum heat requirement from the developed mathematical model could even be calculated for unidentified delamination 1 as 26048.35W/m^2.

5) Time to Identify Defects Analysis on Delaminations: One of the main advantages reported about IRT is the fast rate of scanning to detect defects. Therefore, for the effective application of SPAT in TT mode to analyse defects, the analyses could be made based on the time to identify defects (T) at optimum q. In this approach also, a mathematical model using extracted numerical results is developed to find T of unidentified delaminations. In the similar way to optimum requirement analysis, T could be derived by generalized equations for 0.45mm and 0.6mm depth individually.

T equation for delaminations 1 to 6 could be obtained by:

$$T = 931413333.34s^4 - 43137066.67s^3 + 741506.67s^2 - 5627.75s + 16.41 \quad (3)$$

T equation for delaminations 7 to 12 could be obtained by:

$$T = -106986666.67s^4 + 4576533.33s^3 - 68755.33s^2 + 406.04s - 0.34 \quad (4)$$

From above equations (3) and (4), the delamination 2 and delamination 6 could be identified at optimum q in 1.998sec and 0.3979sec respectively but 0.4765sec and 0.3103sec are required to identify delaminations 8 and 12 respectively. From these results, it is understood that smaller delaminations 2 and 8 need more T than larger delaminations 6 and 12. It is also observed that smaller near-surface delamination 2 needs 1.998sec than 0.4765sec of delamination 8. From these two findings, it is concluded that smaller near-surface delaminations need more T to reach MRTD than deeper delaminations in TT mode. T for unidentified delamination 1 is calculated from the developed mathematical model as 13.0399sec.

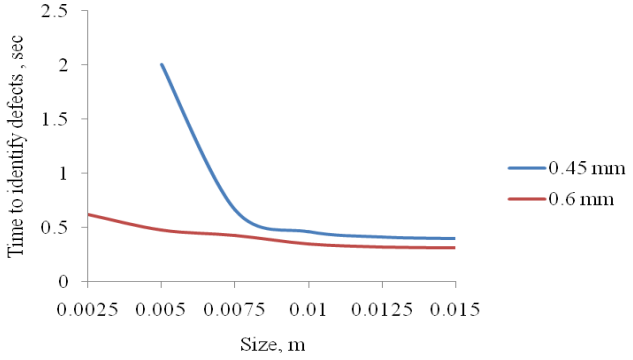

Fig. 12 Compariosn of T for delamiantions 1 to 6 and 7 to 12

B. Analysis of Disbonds

1) Effect of Disbond Size on Applied Heat Flux: The results shown in Figure 13 illustrate that the thermal contrast of disbonds 13 to 18 varies with time. During the initial period, ΔT increases nonlinearly with time and it remains almost constant thereafter. ΔT curves are similar and stacked one above the other for disbonds from 13 to 18. The reason is, the larger disbonds produce more thermal barrier due to increased disbond area by warming up more the surface above disbonds thereby allowing less heat to pass through disbonds to reach the rear surface which is viewed by thermal imager/IR camera. It leads to reduce more the surface temperature of disbonded area than non-disbonded area. It indicates that larger disbonds need less applied q to produce meaningful ΔT to attain MRTD.

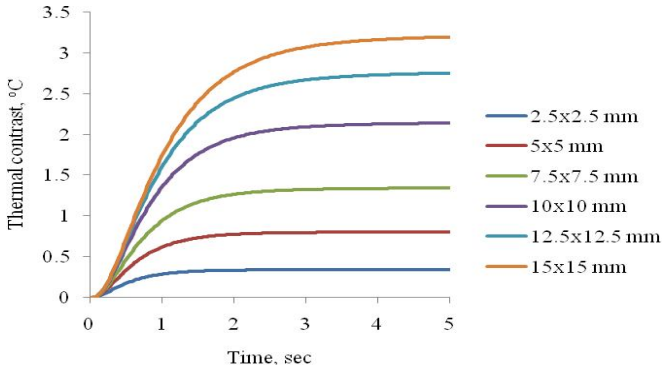

Fig. 13 Thermal contrast curves for disbonds 13 to 18 with time for 16000W/m^2

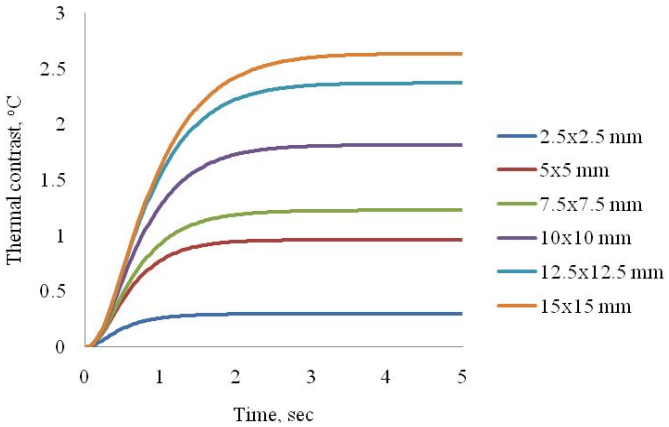

Fig. 14 Thermal contrast curves for disbonds 19 to 24 with time for 9000W/m^2

Figure 14 indicates that ΔT of disbonds 19 to 24 increases nonlinearly with time for the first 2.5 sec and it remains almost constant thereafter. In this case also, ΔT curves are placed one above the other similar to delaminations from 7 to 12. The value of ΔT is less when compared to disbonds 13 to 18, as shown in Figure 13. It is due to the change in thermal conductivity of GRE at 0^o fibre orientation because the disbonds 1 to 6 are located at GRE 90^o fibre orientation and the thermal conductivity of disbond (air) is also less than the thermal conductivity of delaminated material. Therefore, thermal waves are not allowed to pass through disbonds to reach the rear surface is faster than the previous case due to more thermal barrier provided by disbonds. It leads to decrease the surface temperature of disbonded area thereby increasing its ΔT. Hence, deeper disbonds might require slightly more applied q to produce sufficient ΔT which will be investigated in heat requirement analyses.

2) Comparison of Disbonds: Figure 15 shows the comparison between disbonds located at 0.45mm and 0.6 mm depth. It is observed that both near-surface and deeper disbonds produce almost same ΔT up to 1sec but it is less for deeper disbonds thereafter than near-surface disbonds. For example, the disbond 17 produces 1.6011^{o}C as ΔT at 1 sec with 16000W/m^2 but 1.5467 ^{o}C is produced by disbond 23 for the same applied q. Hence, disbonds of same size located at 0.45 mm and 0.6 mm require almost the same q to attain MRTD to identify them. It is slightly more for deeper disbonds.

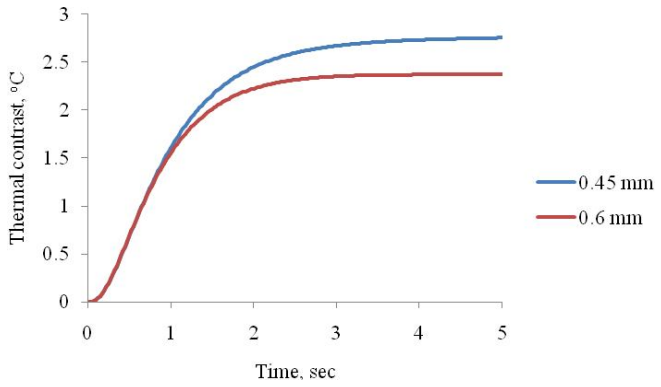

Fig. 15 Comparison of disbonds of 17 and 23 with time for 16000W/m^2

3) Effect of Applied Heat Flux on Fixed Disbond Size: The results shown in Figure 16 demonstrate that ΔT for disbond 15 varies with time for various applied q. ΔT curves are similar and equi-spaced one above the other due to constant increase in applied q. It is observed that disbond 15 produces less ΔT with 10000W/m^2 but it is more when 20000W/m^2 is applied. For example, ΔT at 2 sec is 0.7916°C for 10000W/m^2 and it is 1.5832°C for 20000W/m^2 respectively.

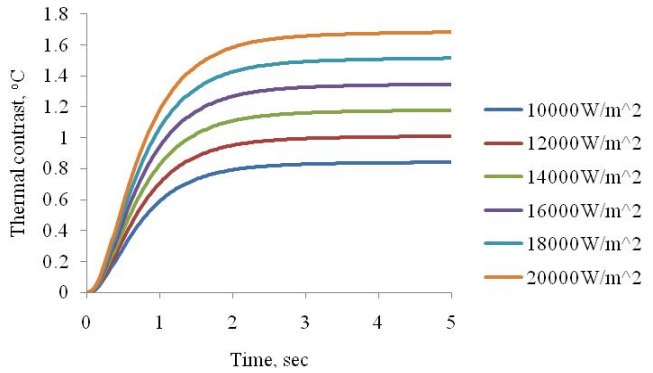

Fig. 16 Thermal contrast curve of disbond 15 with time for various applied q

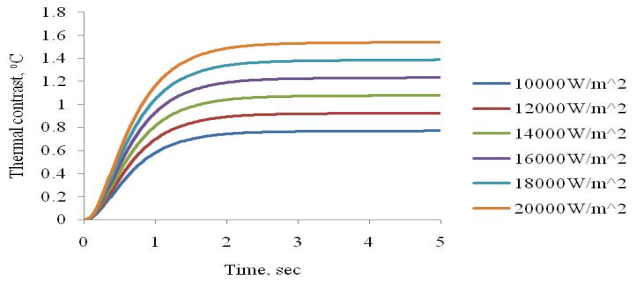

Fig. 17 Thermal contrast curve of disbond 21 with time for various applied q

Figure 17 illustrates ΔT for disbond 21. In this case also, ΔT curves are equi-spaced and they do follow the similar pattern of disbonds from 16 to 18. The results of disbonds 15 and 21 conclude that ΔT of disbond is also directly proportional to the applied q as per Fourier's law of heat conduction.

4) Heat Requirement Analysis on Disbonds: A Figure 18 shows that ΔT at 1 sec for disbonds from 12 to18 varies linearly with q. From results, it is observed that disbond 13 attains more ΔT than the required MRTD with the applied range of q even if it is the same size of delamination 1. Therefore, all disbonds located at 0.45mm depth considered for this investigation could easily be identified. Further development of mathematical models to estimate the optimum q will help the investigation to extend for disbonds more than 15x15 mm which are not considered in this study. Therefore, the optimum heat requirement could be made by extracting equations for each disbond as follows:

$$q = -98798933395894.7s^5 + 4874538669401.36s^4 - 95059626711.32s^3 + 936690133.67s^2 - 4890548s + 12681.10 \quad (5)$$

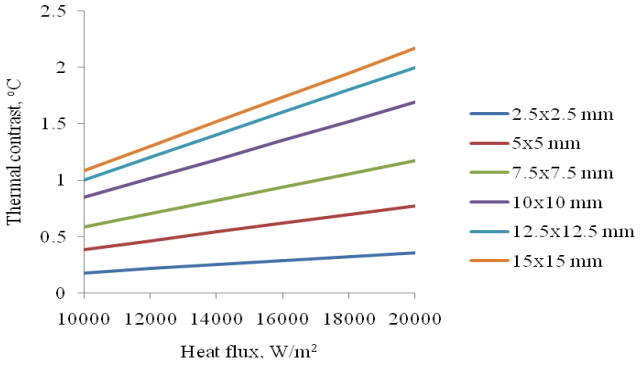

Fig. 18 Thermal contrast curve of disbonds 12 to 18 with q at 1sec

Figure 19 shows that ΔT at 1 sec for disbonds from 19 to 24 varies linearly with applied heat flux. From results, it is observed that disbonds 19 to 24 attain almost same ΔT with the applied q. Hence, the study reveals that the disbonds located at 0.6mm considered for this investigation could easily be identified.

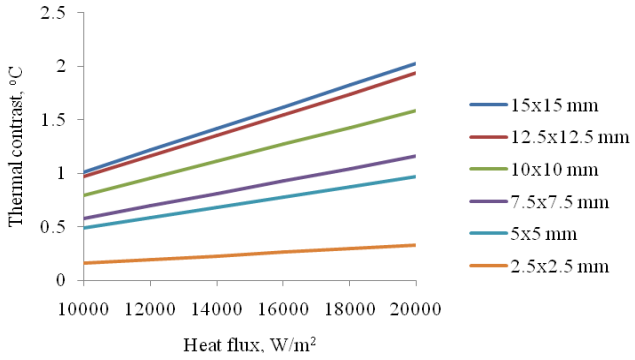

Fig. 19 Thermal contrast curve of disbonds 19 to 24 with q at 1sec

The optimum theoretical heat requirement could be made by extracting equations for each disbond as follows:

$$q = 417951999996.47s^4 - 19385973333.21s^3 + 337905800s^2 - 2666639.81s + 9090.45 \quad (6)$$

From above equations (5) and (6), the disbonds 13 and 18 could be identified at optimum q of 5004.5W/m^2 and 1000W/m^2 respectively but it is 4250W/m^2 for disbond 19 and 850W/m^2 is for disbond 24 to identify them, as shown in figure 20. From these results, it is understood that smaller disbonds 13 and 19 need more q than larger disbonds 18 and 24. It is also inferred that smaller near-surface disbond 13 needs more q to reach the sufficient MRTD than deeper disbond 19.

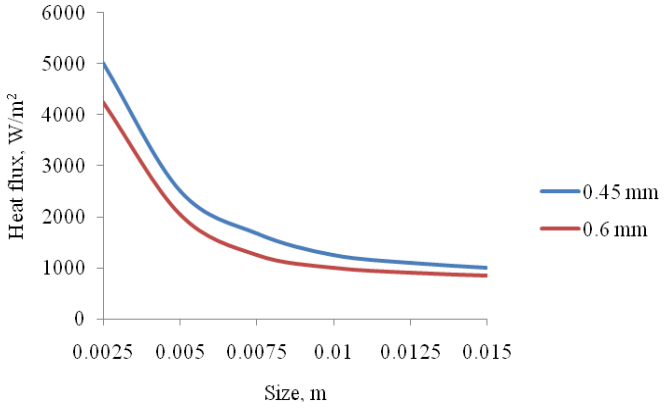

Fig. 20 Compariosn of optimum q requirement for disbonds 13 to 18 and 19 to 24

5) Time to Identify defects Analysis on Disbonds: Similar to delaminations, in this case also, a mathematical model could be developed to calculate T at optimum q as follows:

T equation for disbonds from 13 to 18 could be obtained by:

$$T = 23290666.67s^4 - 1046325.93s^3 + 17429.39s^2 - 128.04s + 0.52 \quad (7)$$

T equation for disbonds 19 to 24 could be obtained by:

$$T = -2592426668.51s^5 + 141806933.41s^4 - 3096181.33s^3 + 33752.91s^2 - 183.04s + 0.55 \quad (8)$$

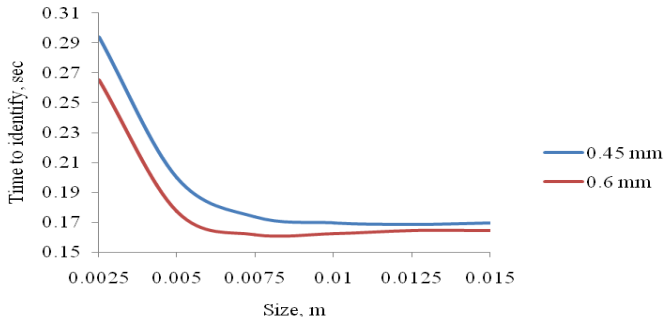

Fig. 21 Compariosn of T for disbonds 13 to 18 and 19 to 24

From above equations (7) and (8), the disbond 13 and disbond 18 could be identified at optimum q in 0.1993sec and 0.1688sec respectively but it is 0.1721sec for disbond 19 and 0.1595sec is for disbond 24 to identify them, as shown in figure 21. From these results, it is observed that smaller disbonds 13 and 19 need more T at optimum q than larger disbonds 18 and 24. The above results reveal that smaller near-surface disbond 13 requires more T to reach MRTD than deeper disbond 19.

C. Comparison of Delaminations and Disbonds

From above results reported from figure 4 to 21, it is observed that both smaller near-surface delaminations and disbonds produce less ΔT with applied q but disbonds respond with increased ΔT than delaminations. The graph shown in Figure 22 shows ΔT of delamination 4 and disbond 16 when 16000W/m^2 is applied. For example, delamination 4 produces 0.2237^{o}C ΔT at 2sec but 1.958^{o}C is produced by disbond 16 at the same 2 sec for the same size and location considered for comparison.

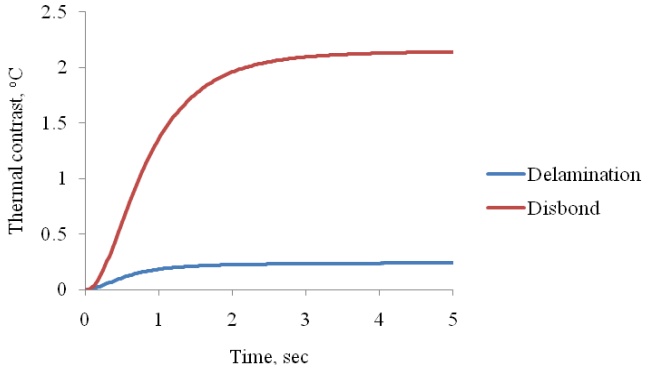

Fig. 22 Thermal contrast curve of delamination 4 and disbond 16 with time for 16000W/m^2

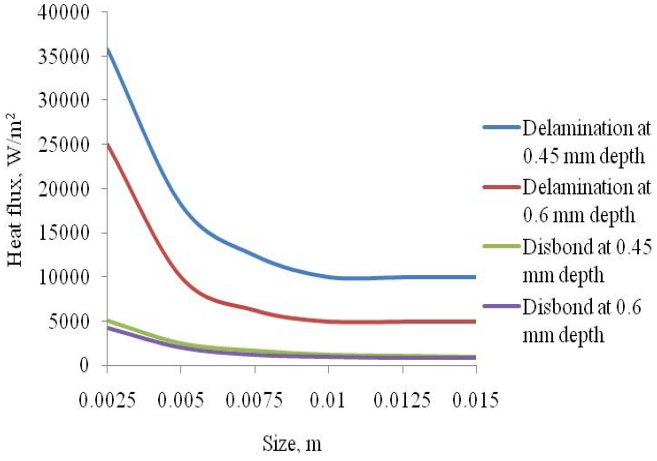

Fig. 23 Compariosn of optimum q for both delamiantions and disbonds

From comparative results, as shown in figure 23, it is inferred that the optimum q to identify disbonds is less than delaminations. It is due to more thermal barrier provided by disbonds to thermal waves than delaminations due to low thermal conductivity of disbonds (air). The optimum q for identifying disbonds located at various depths does come

closer to each other but it is more significant in nature with locations for delaminations located at various depths. In this case, the disbond 16 could be identified with 1250.5W/m^2 but the same size of delamination 4 needs 9998W/m^2. It is due to low thermal conductivity of disbond (Air) than delaminated material.

From results comparison shown in figure 24 for T at optimum q, it is observed that T required to identify disbonds is less than delaminations due to the same reason mentioned for the above case. The variation of T of disbonds located at 0.45 mm is closer to disbonds located at 0.6 mm depth but T makes more significant variation for delaminations located at various depths.

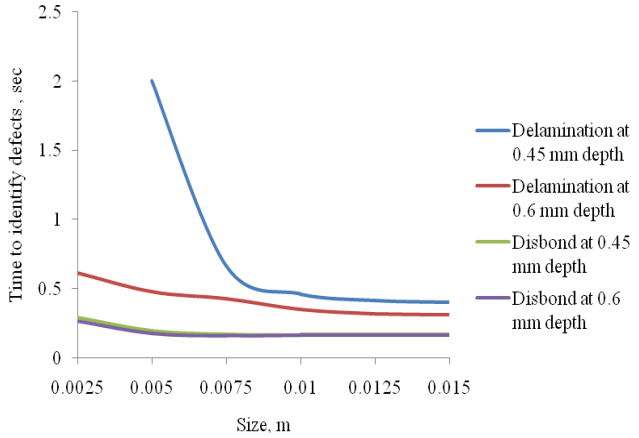

Fig. 24 Compariosn of optimum T for both delamiantions and disbonds

VI. Conclusions

In this study, defects such as delaminations and disbonds present in FML using through-transmission (TT) mode of observation of SPAT method was carried out through developing mathematical models using extracted numerical results to find the optimum heat requirement and time to identify defects. The developed mathematical models allowed to analyse the effect of applied heat flux, time, depth and size of defects for deriving the optimum heat requirement and time to identify defects. Both delaminations and disbonds respond in a different manner by producing its own thermal contrast curve pattern when thermal excitation is applied for numerical simulations. Numerical results based on SPAT in TT mode for analysing defects provide a good defect resolution especially for delaminations; however, numerical results are strongly dependent on surface features and material properties. Generally, smaller and near-surface defects produce less thermal contrast when compared to larger and deeper defects. Nevertheless, disbonds respond more with applied heat flux than delaminations of same size and depth considered. In addition, smaller near-surface delamination 1 needs both q and T more than smaller near-surface disbond 13. The mathematical models provide the optimum heat requirement and time to identify defects at the required MRTD even to identify delamination 1 with 26048.35W/m^2 and time to identify delamination at 13.0399sec. This study shows that the numerical approach based on SPAT method by TT mode of observation could be utilized to analyse defects present in FML effectively.

Nomenclature

q	Heat flux, W/m^2
s	Size of defects, mm or m
ΔT	Thermal contrast, ^{o}C
T	Time to identify defects, sec
t	Time, sec

References

[1] Ad Vlot and Jan Willem Gunnink, "*Fibre Metal Laminates": An Introduction*. Kluwer Academic Publishers. Springer Netherlands, 2001.

[2] ANSYS, *ANSYS Heat Transfer Manual* for Release 10, 2005.

[3] Avdelidis N. P and Almond D.P, "Transient thermography as a through skin imaging technique for aircraft assembly Modelling and experimental results", *Journal of Infrared Phys. Technol*., 2004, Vol. 45. No. 2, pp. 103-114.

[4] Avdelidis N.P, Almond D.P, Dobbinson A, Hawtin B.C, Ibarra-Castanedo C and Maldague X, "Aircraft composites assessment by means of transient thermal NDT", *Progress in Aerospace Sciences*, 2004, Vol. 40, pp 143–162.

[5] Fahr A, Chapman, Forsyth, Poon and Laliberté, "Nondestructive evaluation methods for damage assessment in fiber-metal laminates", *Polymer Composites*, 2000, Vol. 21. No. 4, pp. 568–75.

[6] Guillen and Can, "The influence of cooling rate on the fracture properties of a thermoplastic-based FMLs", *Journal reinforced plastics and composites*, 2002, Vol. 21. No. 8, pp. 749-772.

[7] Hagenbeek M, "Characterisation of Fibre Metal Laminates under Thermo- mechanical Loadings". PhD thesis. Faculty of Aerospace Engineering, 2005, *Delft University of Technology*, pp 224.

[8] Hing Cheng L and Halabe Udaya B, "Finite Element Modeling for Infrared Thermography of GFRP Bridge Decks", *AIP Conference Proceedings, 2008*, Vol. 975. No. 1, pp. 1381-1386.

[9] Ibarra-Castanedo C, Grinzato E, Marinetti S, Bison P, Genest M, Grenier M, Jean-Marc Piau, Bendada A and Maldague X, "Recent progresses in the inspection of aerospace components by infrared thermography" *17th World Conference on Nondestructive Testing*, 2008, *Shanghai, China*, pp.25-28.

[10] Ibarra-Castanedo1 P, Avdelidis N.P, Grinzato G, Paolo G, Sergio M, Claudiu P, Abdelhakim B and Maldague X, "Delamination detection and impact damage assessment of GLARE by active thermography", *International Journal of materials and Product Technology*, 2011, Vol. 41, pp. 5-16.

[11] Krishnapillai M, Jones R, Marshall I.H, Bannister M, and Rajic N, "NDTE using pulse thermography: Numerical modeling of composite subsurface defects", *J. Composite Structures*, 2006, Vol. 75, pp. 241-249.

[12] Lugin S and Netzelmann U, "A defect shape reconstruction algorithm for pulsed thermography", *NDT&E International volume*, 2007, Vol. 40, pp. 220–228.

[13] Mabrouki F, Genest M, Shi G and Fahr A, "Numerical modeling for thermographic inspection of fibre metal laminates", *J. NDT and E International*, 2009, Vol. 42, pp. 581-588.

[14] Maldague X, "*Theory and practice of infrared technology for nondestructive testing*"Wiley-Interscience, *New York*. 453 – 525, 2001.

[15] Meola C, Givanni M.C, Squillace A and Vitiello A, "Non-destructive evaluation of aerospace materials with lock-in thermography" *J. Engineering Failure Analysis*, 2006, Vol. 13. No. 3, pp. 380-388.

[16] Mirela S, Ibrarra-Castanedo, Maldague X, Bendada A, Svaic S and Boras I, "Pulse thermography applied on a complex structure sample: comparison and analysis of numerical and experimental results", *IV conferencia Panamericana de END, Buenos Aires*, 2007.

[17] Muralidhar C and Arya N.K, "Evaluation of defects in axisymmetric composite structures by thermography", *NDT&E International*, 1993, Vol. 26. No. 4, pp. 198-193.

[18] Muzia G, Rdzawski Z.M, Rojek M, Stabik J and Wróbel G, "Thermographic diagnosis of fatigue degradation of epoxy-glass composites", *Journal of Achievements in Materials and Manufacturing Engineering*, 2007, Vol. 24. No. 2, pp. 123-126.

[19] Omar M, Hassan M, Saito K and Alloo R, "IR self-referencing thermography for detection of in-depth defects", *Journal of Infrared Physics and Technology*, 2005, *46*(4), pp 283-289.

[20] Omar M, Haassan M, Donohue K, Saito K and Alloo R, "Infrared thermography for inspecting the adhesion integrity of plastic welded joints", *NDT and E International*, 2006, Vol. 39, pp. 1-7.

[21] Peter linde, Jürgen pleitner, Henk de boer and Jos sinke, "Numerical and experimental simulation of damage behaviour of fibre metal laminates", *24th international congress of the aeronautical sciences*, ICAS 2004.

[22] Qiaojian Huang, Regez Brad, Krishnaswamy and Sridhar, "The influence of disbond defects on Lamb wave testing in GLARE composites" *Proceedings of the SPIE*, 2010, Vol. 7650, pp. 76502P-76502P-8.

[23] Saintey M B and Almond D P, "Defect Sizing by Transient Thermography II: A Numerical Treatment", *Journal of physics. D, Applied physics*, 1995, Vol. 28, pp. 2539-2546.

[24] Speer. and Es-Said. 2004. Applications of an aluminum–beryllium composite for structural aerospace components, *Engineering Failure Analysis*, Vol. 11. No. 6, pp. 895–902.

[25] Timothy B Roth and Ann M. Anderson, "A Light Transmission Based Liquid Crystal Thermography System," *Journal of* Heat Transfer, 2008, Vol. 30. No.1,

[26] Vageswar A, Balasubramaniam K, Krishnamurthy C.V, Jayakumar T and Raj B, "Periscope infrared thermography for local wall thinning in tubes", *NDT&E International*, 2009, *42* (4), pp 275–282.

[27] Vijayaraghavan G K, Majumder M.C and Ramachandran K.P, "Quantitative Analysis of Delaminations in GRP Pipes Using Thermal NDTE Technique", *Journal of Advanced Research in Mechanical Engineering*, 2010, Vol. 1. No. 1, pp.60-68.

ACKNOWLEDGEMENT

The authors would like to acknowledge Dr. Benny Jospeh, Principal, Vimal Jothi Engineering college, Kerla India, for his kind cooperation & support to provide for the valuable guidelines extended to collect literatures about FML. Also, I would like to express my gratitude to Prof. Manikandan .D, Head of the Mechanical Engineering Department, Velammal Engineering college Madurai, India for providing the extended support about Finite element method.

BIOGRAPHICAL NOTES

S.Sundaravalli is currently working as a Faculty in the Department of Mechanical engineering, Roever College of Engineering and Technology, Perambalur, India. An M. Tech in Energy Technolgy from the Podicherry engineering College, Pondicherry, she has around fourteen years of teaching experience and currently pursuing Ph D in the National Institute of Technology, Durgapur, India. She has authored 8 text books, such as Engineering Thermodynmics, Design jigs, fixtures and press tools, Manufacturing technology II, Automobile engineering, Renewable sources of energy etc.,

Dr. M C Majumder is a Professor in the Department of Mechanical Engineering and Member Secretary of the Senate, National Institute of Technology, Durgapur, India. He has a PhD from the Indian Institute of Technology, Kharagpur, India. He has guided many Ph D scholars. His prime area of research is Tribology.

Dr. G.K.Vijayaraghavan is currently working as a Professor in the Department of Mechanical engineering, Roever Engineering College, Perambalur, India. An M. Tech in Machine Design from the Indian Institute of Technology, Madras, he has around Fifteen years of teaching experience and pursed Ph D in the National Institute of Technology, Durgapur, India. He has authored 14 text books including Design of machine elements, Design jigs, fixtures and press tools, Manufacturing technology, Thermal engineering and Mechatronics.